INVESTIGATION OF THE CELLULAR UPTAKE AND CYTOTOXICITY OF

RUTHENIUM(II) POLYPYRIDYL COMPLEXES AS A FUNCTION OF LIPOPHILICITY

by

Matthew Guerrero

Presented to the Faculty of the Graduate School of

The University of Texas at Arlington

Of the Requirements for the Degree of

MASTER OF SCIENCE IN CHEMISTRY

THE UNIVERSITY OF TEXAS AT ARLINGTON

MAY 2022

University of Texas at Arlington. Thank you for your constant love, prayer support and

guidance, and for making me the man I am today.

ABSTRACT

Systematic Variance Of The Number Of Dip Ligands: Effect On Cytotoxicity And Lipophilicity

Matthew Guerrero, M.S

The University of Texas at Arlington, 2021

Supervising Professor: Frederick M. MacDonnell

Ru(II) polypyridyl complexes have been one of the focal points of investigation for inorganic anti-cancer drugs, as they are robust enough to remain chemically intact in vivo and many show potent cytotoxicty. In particular, the RPC $[Ru(dip)_3]^{2+}$, where dip is 4,7-diphenyl-1,10-phenanthroline, is noted for its high cytotoxicity (IC_{50} ~2-5 μM) across a broad spectrum of cancer cell lines and more recently has been implicated as targeting microtubules, which is an unusual target for metal-based drugs. While the cellular uptake for $[Ru(dip)_3]Cl_2$ is among the highest seen for RPCs, its solubility in water or buffer is limited and problematic. In order to obtain clear aqueous solutions, it is first necessary to dissolve the complex in DMSO and then dilute it into water (or buffer) and more recent work has shown this solution to be colloidal. In contrast, the RPCs $[Ru(bpy)_3]Cl_2$ and $[Ru(phen)_3]Cl_2$ are freely soluble in water or buffer but show low cellular uptake and low cytotoxity (IC_{50} >50 μM). In an effort to examine how the cellular uptake and compartmentalization are affected by the presence of the dip ligand in trischelate ruthenium polypyridine complexes (RPCs), the following series of RPCs were synthesized: $^+$, $[Ru(bpy)_3]^{2+}$, $[Ru(phen)_3]^{2+}$, $[Ru(bpy)_2dip]^{2+}$, $[Ru(phen)_2dip]^{2+}$, $[Ru(dip)_2bpy]^{2+}$, $[Ru(dip)_2phen]^{2+}$, and $[Ru(dip)_3]^{2+}$ (bpy = 2,2'-bipyridine), with the two heteroleptic bpy complexes being unknown prior to this work. After conversion to the chloride salt, all of the

RPCs were assayed for their LogP, cytotoxicity, cellular uptake, and subcellular localization in MCF-7 and H-358 cell lines.

We were able to show a systematic increase in the logP values with the number of dip ligands and homologues with phen ligands generally more lipophilic than those with bpy ligands. Moreover, a substantial difference in the logP values depending on the nature of the aqueous phase was observed. In octanol/water (o/w) measurements, $logP_{o/w}$ values tended to be higher than when measured in octanol/PBS buffer (o/b), which could be a salting out effect, however for [Ru(dip)phen]2+, the value of $logP_{o/w}$ jumps from -1.1 to +1.2 for $logP_{o/b}$! In this case, the increase is clearly due to more than simple ionic strength effects. Ultimately the aqueous solubility of the RPCs is good for all excepting [Ru(dip)$_3$]Cl$_2$, and the bis dip substituted RPCs [Ru(dip)$_2$bpy]Cl$_2$ and [Ru(dip)$_2$phen]Cl$_2$ showing an optimal combination of aqueous solubility, cellular uptake and cytotoxicity. Investigations into the subcellular localization reveal that these two RPCs also predominantly localize in the cytoskeletal fraction of the cell lysates suggesting they also target microtubule function as their mechanism of action.

In this thesis, Chapter 1 is a review of the RPCs as potential anti-cancer drugs and an update of their role in targeting microtubules. Chapter 2 describes the synthesis and characterization of [Ru(bpy)$_2$dip]$^{2+}$and [Ru(dip)$_2$bpy]$^{2+}$ and the measurements of the lipophilicity of these complexes via determination their partition coefficients (LogP) by utilizing the shake-flask method in octanol/water and octanol/buffer. Chapter 3 describes the cellular assays and measurements and correlates these data with the lipophilicity and structural characteristics of the RPCs.

TABLE OF CONTENTS

4T1	Mice breast cancer cell line
A-549	Human lung adenocarcinoma
bpy	2,2'-bipyridine
CD_3CN	Deuterated acetonitrile
$(CD_3)_2SO$	Deuterated dimethyl sulfoxide
Cisplatin	cis-Diamminedichloroplatinum (II)
Cl^-	Chloride
d	doublet
dd	doublet of doublets
dip	4,7-diphenyl-1, 10-phenanthroline
DMF	Dimethylformamide
DMSO	Dimethyl sulfoxide
DNA	Deoxyribonucleic acid
ε	Extinction coefficient
ER	Endoplasmic Reticulum
FBS	Fetal bovine serum
FDA	Food and Drug Administration

^{1}H	Proton
H-358	Human non-small cell lung carcinoma
IC$_{50}$	Half maximal inhibitory concentration
ICP-MS	Inductively coupled plasma mass spectrometry
KP1019	Indazolium trans-[tetrachlorobis(1H-indazole)ruthenate(III)]
L-L	Bidentate ligand
LC-MS	Liquid chromatography mass spectrometry
LiCl	Lithium Chloride
LogP	Partition Coefficient
m	Multiplet
MCF-7	Human mammary tumor cell line
MSA	Microtubule stabilizing agent
MT	Microtubule
MTT	3-(4,5-Dimethylthiazol-2-yl)-2,5-diphenyltetrazolium bromide
NAMI-A	[ImH][trans-RuCl4(DMSO)(Im)]
NMR	Nuclear magnetic resonance
o/b	Octanol/Buffer
o/w	Octanol/Water

PBS   Phosphate buffered saline

phen   1,10-phenantroline

Pt   Platinum

RPC   Ruthenium polypyridyl complex

Ru   Ruthenium

s   singlet

t   triplet

UV   Ultraviolet

Vis   Visible

Chapter 1: Background for the Family of Ruthenium Complexes

The success of cisplatin (cis-Pt(NH$_3$)$_2$Cl$_2$) in the treatment of human cancers has spurred interest in developing other transition-metal complexes for cancer therapies.[1,2] Of the multitude of possible metallodrugs, ruthenium(II) polypyridyl complexes (RPCs) are among the most widely studied outside of platinum complexes. Unlike cisplatin, RPCs do not lose ligands and form new metal-ligand bonds with biological substrates, instead the entire complex cation is the active drug which binds to and interacts with cellular target via non-covalent interactions. RPCs are actively being explored as photosensitizers for photodynamic therapy (PDT), however many RPCs are inherently cytotoxic and thus could be used for a systemic cancer treatment/therapy as the location of the tumor may not be known. At present, only one RPC has advanced to clinical studies. TLD-1433 is in Phase II clinical trials as a PDT agent for treatment of bladder cancer.[12] Passing the Phase I studies shows that this RPC was ruled safe for further human studies, albeit that the application was intravesical and instilled into the bladder.[12] Much of this is due to the relatively early stage of their investigation as therapeutics and the dearth of supporting studies on animal toxicity, pharmacodynamics and pharmacokinetics.

Chemical Stability in vivo

One important reason for their study is that RPCs are exceptionally stable and kinetically inert, such that concerns about the complex cation fragmenting or otherwise decomposing in the biological milieu are unwarranted.[27-29] For example, [Ru(phen)$_3$]$^{2+}$ can survive boiling in concentrated acids or alkalis,[24] and has been used as a digestive marker for ruminant animals as it is not absorbed and passes through the animal.[24-26] Moreover, rats and mice given

intraperitoneal injections of radiolabeled [^{106}Ru(phen)$_3$][ClO$_4$]$_2$ excreted this cation fully intact in the urine in about 12 h. These complex cations should be considered as metabolically robust as the polypyridyl ligands that they possess. This stability considerably simplifies examination of the RPCs molecular mechanism of action as we can generally rule out metabolites or decomposition products as the active components.   It should also be noted that the tris chelate RPCs, such as [Ru(phen)$_3$]$^{2+}$, are chiral (propeller molecules with D_3 point group symmetry) and for the most part have been studied as a racemic mixture of Λ and Δ enantiomers. No attempt to work with enantiopure complexes was made in this work.

Inhibition and mouse toxicity studies show that certain RPCs, especially those which are more highly hydrophilic, to be potent inhibitors of acetylcholine esterase (AChE) leading to maximum tolerated doses (MTDs) in mice as low as 6.6 mg RPC/kg mouse body weight. This is highly variable, and some other, more lipophilic RPCs had MTDs over 160 mg/kg.[15,16] In cases in which enantiopure RPCs were used, such as Δ and Λ-[Ru(phen)$_3$]$^{2+}$, the Λ enantiomer was twice as toxic as the other enantiomer.[17,18]

Cellular uptake and subcellular targets

Some early studies of RPC cellular uptake revealed that uptake is correlated with lipophilicity in many instances, and that in most such cases the uptake is via passive diffusion.[4,39] For many years, DNA was the presumed cellular target of cytotoxic RPCs as selective DNA binding and damage had been demonstrated in numerous cell-free studies.[32,40,41,42,43,44,45] Some early exceptions were [Ru(dip)$_3$]$^{2+}$ and [Ru(dip)$_2$(dppz)]$^{2+}$ (see Figure 1) both of which show good cellular uptake relative to less lipophilic analogues and the latter was observed to be concentrated outside the nucleus in a fluorescent microscopy analysis.[4] [Ru(dip)$_3$]$^{2+}$ is a potent

cytotoxin in numerous malignant (H358, MCF7, CCL228, HL60, B16, MDA-MB-231, A549, Jurhkat, ML2, SF) and non-malignant (MCF10a) cell lines with IC_{50} values consistently ranging between 1 and 4 µM irrespective of the cell type.[20-23]   The mitochondria has been implicated as the cellular target for $[Ru(dip)_3]^{2+}$ and other RPCs in several studies, however recently Alatrash *et. al.* has shown that $[Ru(dip)_3]^{2+}$ can also target microtubules in vitro and in live cells.[4,10,17,47,48,49,50]

In a detailed study, $[Ru(dip)_3]^{2+}$ was shown to promote tubulin polymerization *in vitro*, and, more significantly, to bind MTs *in vivo* (live cells) in a manner which induces massive changes to the MT dynamics.[17] This MT disrupting activity correlates with the observed cytotoxicity and supports this as the dominant apoptotic mechanism of action.

Moreover, in treated cells that have been fractionated and examined for ruthenium content by ICP-MS, over 80% of the ruthenium content in the cytoskeletal fraction (vs. mitochondrial/ER/Golgi; nuclear, and cytosolic fractions) as is shown in Figure 1. This is not a general feature of RPCs as the smaller and more hydrophilic $[Ru(phen)_3]Cl_2$, which rarely shows any cytotoxicity below 50 µM,[20] is much more evenly distributed in the cellular fractions. As seen in Figure 1A, the cellular uptake of the two RPCs differs considerably and the data at 4 °C supports passive diffusion as the mechanism, as the uptake in nearly identical to that at 37 °C.
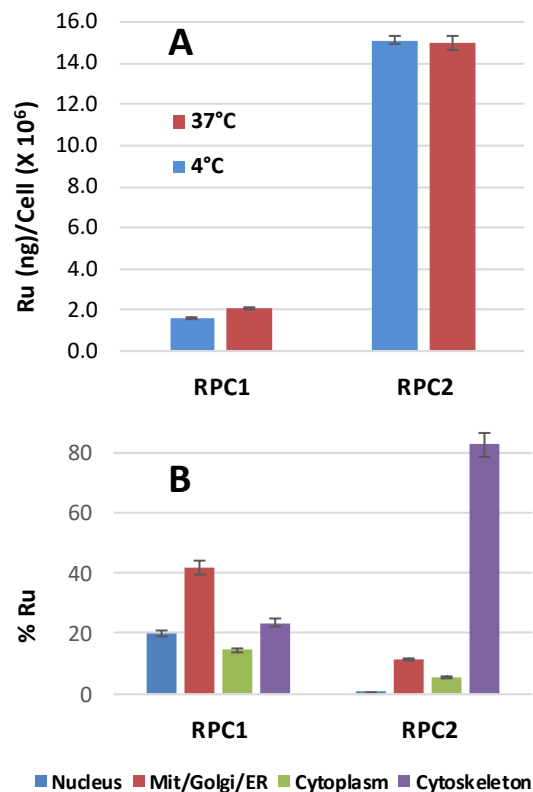
Figure 1. Ru content in whole (top) and fractionated (bottom) H358 cells. (A) Mass of ruthenium in ng per million cells for H358 cells incubated with 20 μM of **RPC1** or **RPC2** for 12 h at 37°C C or 4°C. (B) Percent ruthenium found in four different fractions of H358 cells (nucleus, cytosol, mito/Golgi/ER, cytoskeleton). The cells were fractionated using a QIAGEN Compartment Kit and Ru ion content was analyzed using ICP-MS.[17]

This cytoskeletal target for RPCs has some far-reaching implications. MTs are highly dynamic polymers of tubulin, which are crucial in maintaining the structure of the cell and are involved in processes critical to cell survival (e.g., intracellular transport and cell division).[10–12] As such, MTs represent an attractive and common target for anticancer therapeutics. Two general classes of drugs exist that are microtubule targeting agents (MTAs). Microtubule destabilizing agents (MDAs) inhibit polymerization and microtubule stabilizing agents (MSAs) which promote

polymerization. Paclitaxel, docetaxel, and vinorelbine are three natural products or semi-synthetic analogues of natural products that are clinically used MTAs and function via the disruption of normal MT dynamics (polymerization and depolymerization). Paclitaxel is a known microtubule stabilizing agent used for polymerization. Docetaxel and Vinorelbine are utilized as a chemotherapeutic to prevent microtubule depolymerization. As seen from their chemical structures in Figure 2, these are incredibly complex organic molecules with numerous interlocking rings and stereocenters. The natural supply of some of these natural products, particularly for the taxanes, is limited and synthetic routes for their preparation can exceed 40 steps.[12,13,15,16] In contrast, kilogram quantities of [Ru(dip)$_3$]Cl$_2$ or many RPCs can be made in short order from rather common commercially available ligands. While it is premature to say that [Ru(dip)$_3$]Cl$_2$ can supplant any of these natural products, it is promising that this rather simple molecule shows similar bioactivity and we have only begun to explore RPC analogues which may have even better performance.
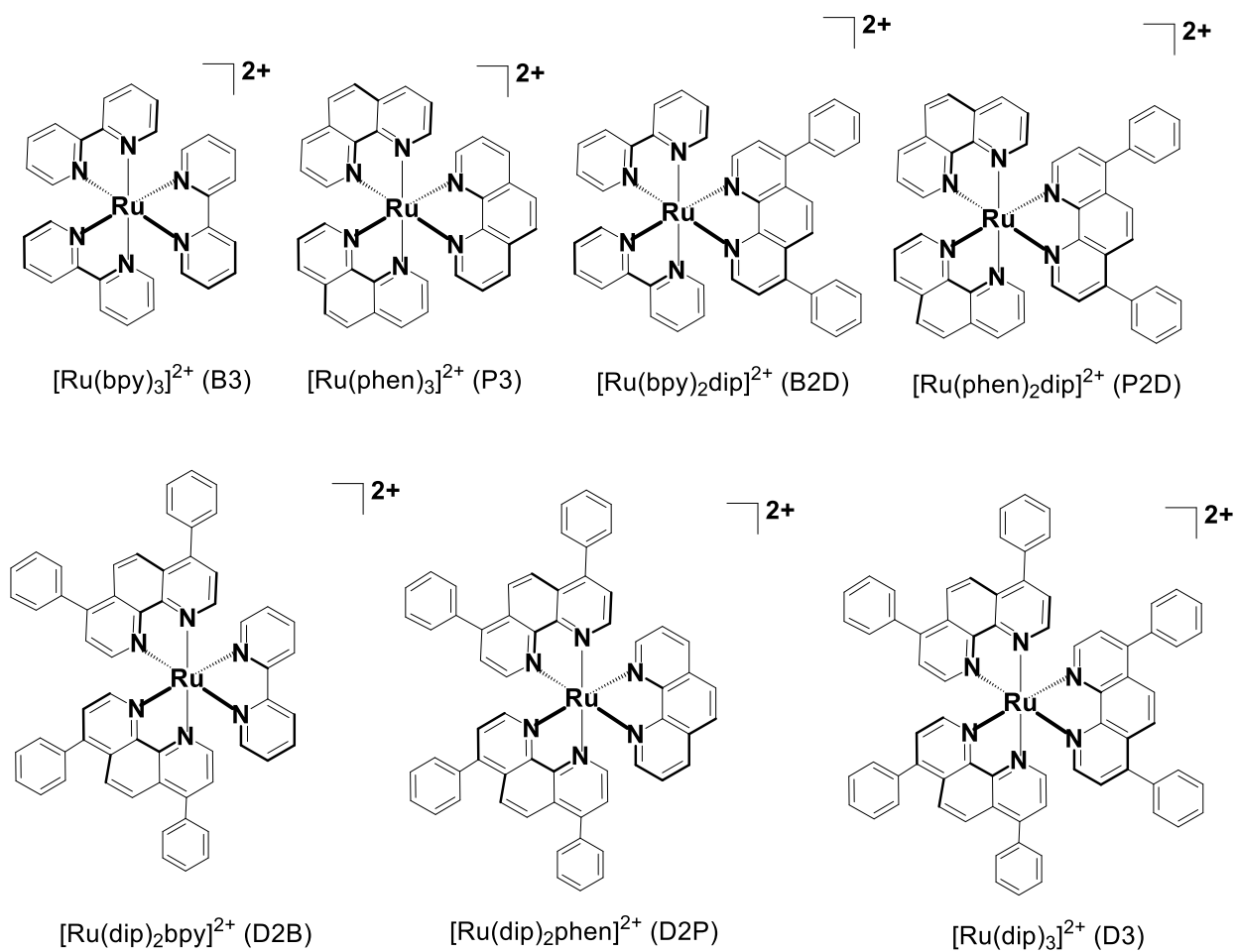

Paclitaxel   Docetaxel   Vinorelbine
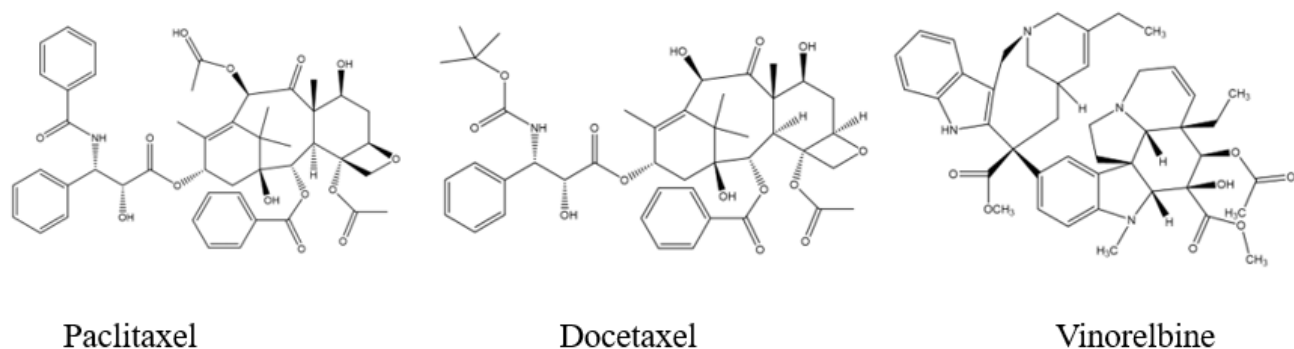
Figure 2. Semi-synthetic and natural product MTAs.

Our challenge with the use and study of $[Ru(dip)_3]Cl_2$ in biological assays is its sparing solubility in aqueous solution. It is not possible to directly dissolve this complex in water or buffer. Instead, the complex is dissolved into DMSO or MeCN to form a concentrated (i.e. 2 mM) stock solution which is then diluted into water or buffer, yielding clear red-orange solutions, even when diluted such that the DMSO or MeCN concentration is less than 1 % v/v. This technique is also used for the even more water insoluble $[Ru(dip)_3][PF_6]_2$ salt, generally with similar success. Recent reports that this complex actually forms colloids under such conditions reveal clusters of ~50 nm spheres by TEM.[46]

In this work, we move to circumvent the solubility issues associated with $[Ru(dip)_3]Cl_2$ by sequentially replacing the dip ligands with the more hydrophillic phen and bpy ligands. While this substitution is expected to alter the RPC lipophilicity (logP), it is unknown how these substitutions will affect the cellular uptake, subcellular localization, and cytotoxicity. Our goal is to obtain a $[Ru(dip)_3]Cl_2$ analogue with enhanced aqueous solubility but with similar or improved uptake, specificity, and cytotoxicity. Herein we report the syntheses of the following analogues, $[Ru(dip)_2bpy]Cl_2$ and $[Ru(bpy)_2dip]Cl_2$, our study of the following family of RPCs (shown in Figure 3) with respect to $logP_{o/w}$, $logP_{o/b}$, as well as cellular uptake, subcellular localization, and cytotoxicity in two malignant human cell lines, H358 and MCF7. Figure 3 also shows the shorthand notation used to refer to the RPCs in this work.

[Ru(bpy)₃]²⁺ (B3)　　[Ru(phen)₃]²⁺ (P3)　　[Ru(bpy)₂dip]²⁺ (B2D)　　[Ru(phen)₂dip]²⁺ (P2D)

[Ru(dip)₂bpy]²⁺ (D2B)　　　[Ru(dip)₂phen]²⁺ (D2P)　　　[Ru(dip)₃]²⁺ (D3)

Figure 3. Chemical structures ruthenium polypyridyl complexes explored in this work.

Chapter 2. Synthesis of [Ru(dip)$_2$(bpy)]Cl$_2$ and [Ru(bpy)$_2$(dip)]Cl$_2$

<u>Introduction</u>

The synthesis of the heteroleptic [Ru(dip)$_2$(bpy)]Cl$_2$ and [Ru(bpy)$_2$(dip)]Cl$_2$ was followed off of a procedure developed by Sullivan and Barton et. al. Sullivan was the first to report the synthesis of [Ru(bpy)$_2$Cl$_2$] and Barton was the first to conduct this synthesis with the dip ligand, which resulted in [Ru(bpy)$_2$Cl$_2$].[10,11] Myself among many others, including those who have worked in our lab previously have utilized these well renowned synthetic methods to consistently create the [Ru(dip)$_2$]Cl$_2$, [Ru(bpy)$_2$]Cl$_2$, and [Ru(phen)$_2$]Cl$_2$ starting materials. These procedures have been utilized since the 1970s and early 1990s and have been known to produce clean products in good yield.[10,11]

<u>Experimental</u>

Chemicals

The solvents and reagents used were reagent grade and utilized as received. Ruthenium (III) chloride hydrate was purchased from Pressure Chemical Company. 2'2-bipyridine (bpy), 4,7-diphenyl-1,10-phenanthroline (dip), ammonium hexafluorophosphate (NH$_4$PF$_6$), tetrabutyl ammonium chloride hydrate, lithium chloride (LiCl), acetone, methanol, ethanol, acetonitrile, and octanol were all purchased from Sigma Aldrich. PBS buffer 10X was procured from Bio-Rad. The PBS had to be diluted before usage 10-fold using Millipore water resulting in a normal 1X PBS buffer (1.37 M NaCl, 27 mM KCl, 100 mM Na$_2$HPO$_4$, 18 mM KH$_2$PO$_4$, pH 7.2). The two homoleptic complexes [Ru(dip)$_3$]Cl$_2$ and [Ru(bpy)$_3$]Cl$_2$ were synthesized based off of their respective literature and their spectra are shown in appendix Figures 1 and 2.[10,11]

^{1}H NMR

All ^{1}H NMR spectra were attained by using a JEOL Eclipse Plus 300 MHz Spectrometer by using $(CD_3)_2SO$ or $(CD_3)_2CO$ as the solvents.

LC-MS

All LC-MS studies were conducted on a Shimadzu UFLCXR LC-MS 2020. Minimal amounts of methanol and acetonitrile were used to dissolve the samples. Instrument parameters were; no column, 1 µL injection volume, 0.25 mL/min flow rate, 2 minute runtime, 100% acetonitrile mobile phase, 150-1500 m/z scan mode, 1500 u/sec scan speed. $[Ru(dip)_3]Cl_2$ and $[Ru(bpy)_3]Cl_2$ were implemented as pre and post run standards for the LC-MS procedure.

Synthesis

Ru(dip)$_2$Cl$_2$

$Ru(dip)_2Cl_2$ was made in a similar manner to $[Ru(bpy)_2]Cl_2$, as described by Sullivan et al..[10] To begin, 0.56 g (1.68 mmol) of dip, 0.2 g (0.7 mmol) of $RuCl_3 3H_2O$, 0.12 g (2.8 mmol) of LiCl were placed in a 2-neck round bottom flask along with 20 mL dimethylformamide. LiCl was utilized to help force a cis product while the DMF was utilized as a reducing agent. The mixture was left to reflux for 24 hours under nitrogen with stirring. Upon cooling, the resulting purple mixture was placed in a beaker along with 60 mL of cold acetone to help with precipitation and yield. The resulting purple precipitate was filtered in a Buchner funnel with a fritted disc, and then washed with copious amounts of water (until the filtrate was nearly clear),

then dried in a vacuum oven at 80 °C for 1 hour. The product was redissolved in acetone (50 mL) and 40 mL water added to initiate another precipitation. This precipitate was again filtered and washed with excess water until the filtrate became clear. This final precipitate was again dried for a period of 4-6 hours at 80 ˚C. Yield 0.740g (92 %). ^{1}H NMR ((CD)$_3$)$_2$SO); 10.39 (d, 2 H), 8.16-8.22 (dd, 4 H), 7.98 (dd, 4 H), 7.89 (t, 5 H), 7.69 (t, 4 H), 7.60 (t, 2 H), 7.45-7.59 (m, 11 H), 7.35 (d, 2 H).

[Ru(dip)$_2$bpy]Cl$_2$

A 200 mL RBF was charged with 100 mg (0.1 mmol) Ru(dip)$_2$Cl$_2$ and 18 mg (0.1 mmol) bpy and with 60 mL of ethanol and 50 mL of water. The mixture was left to reflux overnight. After cooling, the resulting solution was filtered, and the filtrate was concentrated via rotary evaporator until 30-40 mL remained. This solution was filtered again by using a medium porosity glass frit to remove any remaining starting material. The filtrate was then evaporated to dryness. The red solid was washed suspended in x mL of ice-cold acetone and sonicated for 10 min sonication to dissolve any remaining excess Ru(dip)$_2$Cl$_2$. The final dark red solid product was collected via suction filtration, washed with ice cold acetone, then dried for a period of 4-6 hours at 80 ˚C. This crude product was purified via silica chromatography (methanol/acetonitrile). The chromatography produced 3 major bands, with the first band being a dark purple color, the second band being a dark red color and the third band being an orange color. The second band was left to evaporate then collected for ^{1}H NMR.[14] Yield 27 mg (38%). Anal. calcd C$_{58}$H$_{42}$Cl$_2$N$_6$Ru·2H$_2$O : C, 67.57%; H, 4.50%; N, 8.15%, found: C, 67.86%; H, 4.04%; N, 8.11%; ^{1}H NMR (CD$_3$CN, 300 MHz): δ= 8.92 (d, 2 H), 8.31 (d, 2 H), 8.24 (s, 4 H),

8.21 (d, 2 H), 8.20 (t, 2 H), 7.92 (d, 2 H), 7.83 (d, 2 H), 7.73 (d, 2 H), 7.56-7.71 (m, 20 H), 7.50 (t, 2 H); ESI-MS (m/z): 461 [M-Cl$_2$]$^{2+}$

[Ru(bpy)$_2$dip]Cl$_2$

To begin this synthesis, 100 mg (1mmol) of [Ru(bpy)$_2$]Cl$_2$ and 70 mg (1mmol) of dip were placed in a 200 mL round bottom flask along with 60 mL of ethanol and 50 mL of water. The reactants were left to reflux overnight. The next day the reaction was left to cool to room temperature, then the resulting solution was filtered, and the filtrate was concentrated via rotary evaporator until 30-40 mL remained. This solution was filtered again by using a medium porosity glass frit in an attempt to remove any remaining starting material. The filtrate was then evaporated until dryness. After drying, ice cold acetone was placed in a beaker containing the dark red product, then was sonication for 10 minutes to better dissolve any remaining excess reactant that did not attach to the product. The final dark red solid product was collected via suction filtration, washed excessively with ice cold acetone, then dried for a period of 4-6 hours at 80 ˚C, then purified via silica chromatography (methanol/acetonitrile). The chromatography produced 2 major bands, with the first band being a dark red color, the second band being an orange color. The second band was left to evaporate then collected for ^{1}H NMR. Yield 45 mg (40%). Anal. Calcd for C$_{44}$H$_{34}$Cl$_2$N$_6$Ru·2H$_2$O: C 61.83, H 4.48, N 9.83, found: C 61.25, H 4.31, N 9.62; ^{1}H NMR (CD$_3$CN, 300 MHz): δ= 8.55 (t, 4 H), 8.17 (s, 2 H), 8.12 (d, 2 H), 8.09 (t, 2 H), 8.01 (t, 2 H), 7.85 (d, 2 H), 7.66 (d, 4 H), 7.54-7.63 (m, 10 H), 7.44 (t, 2 H), 7.26 (t, 2 H); ESI-MS (m/z): 373 [M-Cl$_2$]$^{2+}$.

Partition Coefficient (LogP) Determinations

       The lipophilicity of the ruthenium complexes was determined via the shake-flask method using octanol and PBS (1X) buffer (o/b) or octanol and water (o/w). To begin this assay, 33.3×10^{-5} M of solute was placed in a 50 mL centrifuge tube with 10 mL of octanol and 10 mL of buffer. The concentration and the volume remained the same for each complex tested, and only the amount of complex added was changed slightly for each different ruthenium complex. For example, when conducting this assay with $[Ru(dip)_2bpy]Cl_2$, 6.6 mg of the complex was added. This value differed slightly when the $[Ru(bpy)_2dip]Cl_2$ complex was used, as only 5.4 mg was added into solution. These same ratios were also utilized when determining the $LogP_{o/w}$ with 10 mL of octanol and 10 mL of water. Both saturated phases were shaken manually for 30 minutes at room temperature and then left to equilibrate for 24 hours. After the equilibration period, the concentration of the complex in each solvent was determined by measuring the absorbance at 460 nm in a 1 cm quartz cuvette. For simplicity, the molar extinction coefficient was assumed to be unchanged by the solvent. The LogP, is calculated via the formula:

$$\log P = \log ([solute]octanol /[solute]buffer \text{ or water})$$

       $[Ru(bpy)_2Cl_2]$ and $[Ru(dip)_2Cl_2]$ were prepared following the method of Sullivan et. al. as starting materials for the heteroleptic products. Displacement of the chloride ligands and coordination of the third diamine chelate ligand results in the substitutionally saturated and kinetically inert products, such as $[Ru(bpy)_2dip]Cl_2$, and $[Ru(dip)_2bpy]Cl_2$. It is common for these products to be initially isolated as the hexafluorophosphate salts, i.e., $[Ru(bpy)_2dip][PF_6]_2$ and $[Ru(dip)_2bpy][PF_6]_2$, and then metathesized to the chloride salt. Attempts to follow this

route always showed retention of some PF_6^- anion, as the chloride salt of these cations does not cleanly precipitate from acetone solution. In order to work around this challenge, the initial product was isolated as the chloride salt and purification was affected via silica gel chromatography in a 50:50 mixture of methanol and acetonitrile. This process was able to produce significantly cleaner and larger yields.

The structure of $[Ru(bpy)_2dip]Cl_2$, and $[Ru(dip)_2bpy]Cl_2$ were confirmed by ^{1}H NMR using deuterated acetonitrile and dimethyl-sulfoxide and are shown in Figures 4 and 5 as well as in the appendix section. The peak assignments made were using a combination of data. First, the point group symmetry for the homoleptic tris complexes is D_3, and thus the resulting NMR spectra show only few peaks per complex. For the heteroleptic RPCs, this symmetry is lowered to C_2, resulting in a more complicated NMR spectra. That said, the ^{1}H NMR for the homoleptic complexes in the same solvents does provide aid in assigning the peaks for the ligand with C_2 symmetry. In addition, COSY spectra were obtained to correlate which peaks were correlated (adjacent) on the ligands.   The phenyl groups located on the dip ligands did not give cleanly resolved peaks and instead come as a multiplet centered at 7.6 ppm. ESI-MS and CHN analysis were also obtained and consistent with the proposed structure. The calculated m/z value for $[Ru(bpy)_2dip]^{2+}$ is 373 which is observed in the ESI-MS. Similarly, the calculates m/z of 461for $[Ru(dip)_2bpy]^{2+}$ is observed in the ESI-MS. Correspondingly, the observed CHN analyses for both $[Ru(bpy)_2dip]^{2+}$ and $[Ru(dip)_2bpy]^{2+}$ match the calculated values, and these were shown above in the synthesis section.

Results and Discussion
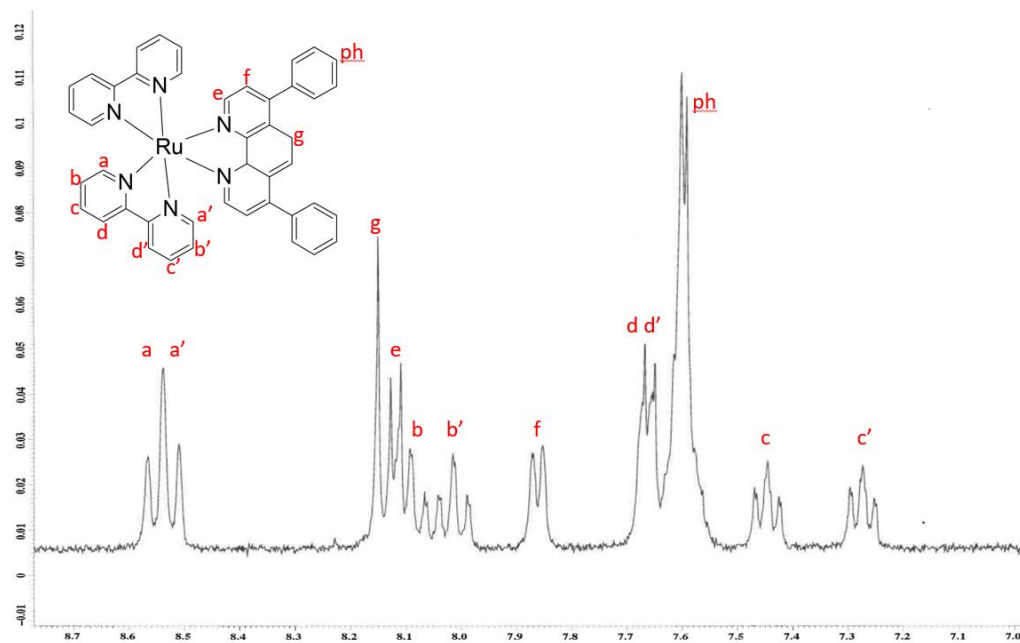
Figure 4. ^{1}H NMR labeling of the [Ru(bpy)$_2$dip]$^{2+}$ complex. Ph represents the phenyl group attached to the dip ligand. Letters a-d and a'-d' represent the bpy ligand protons while the letters e-g represent the dip ligand protons. ^{1}H NMR solvent: CD$_3$CN
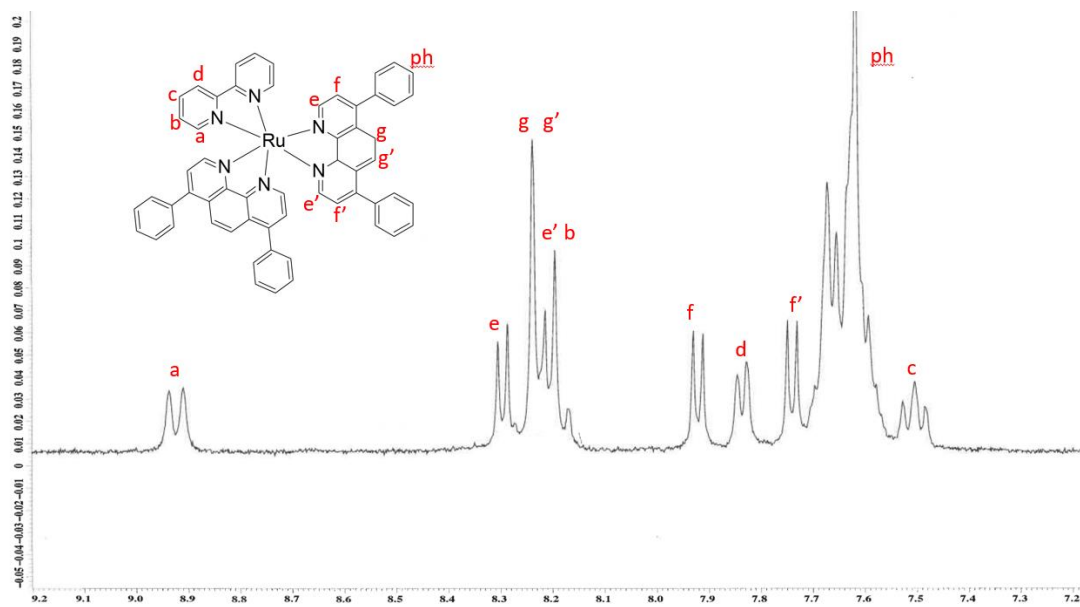
Figure 5. ^{1}H NMR labeling of the [Ru(dip)$_2$bpy]$^{2+}$ complex. Ph represents the phenyl group attached to the dip ligand. Letters a-d represent the bpy ligand protons while letters e-g and e'-g' represent the dip ligand protons. ^{1}H NMR Solvent: ((CD$_3$)$_2$S=O)

14

The partition coefficients for the two new complexes were obtained by utilizing the shake-flask method described in the Experimental section. These data sets and those obtained for the other RPCs shown in Figure 2 are compiled in Table 1. Both $LogP_{o/w}$ and $LogP_{o/b}$ are reported as well as the difference of these two measurements. In most pharmacological studies LogP is measured in octanol/water mixtures however we have previously shown that for charged solutes, i.e. cationic RPCs, this value can be altered dramatically by the presence and nature of the counterions in the buffer system.[17]

For the homoleptic complexes, the logP (lipophilicity) increases $[Ru(bpy)_3]Cl_2 <$ $[Ru(phen)_3]Cl_2 < [Ru(dip)_3]Cl_2$, regardless of the water of buffer system. This is sensible in that bpy has the smallest amount of aromatic area and is the most water soluble of the three ligands, while dip has the most aromatic surface area and is the most lipophilic ligand. In the heteroleptic complexes, the lipophilicity seems to be most dramatically affected by the number of dip ligands present and then as a secondary affect by phen over bpy. In Table 1, the RPCs are listed from most lipophilic to least (top to bottom) and follow the anticipated order of the basis the number of dip ligands and phen or bpy ligand. Notably the order is the same regardless of the water or buffer solvent.

Table 1. Entire family of ruthenium polypyridyl complexes and their respective LogP values in buffer/octanol and water/octanol systems. LogP$_\delta$ shows the difference between buffer/octanol and water/octanol systems.

RPC	LogP$_{o/b}$	LogP$_{o/w}$	LogP$_\delta$
[Ru(dip)$_3$]Cl$_2$ (D3)	1.9	1.4	0.5
[Ru(dip)$_2$bpy]Cl$_2$ (D2B)	0.92	0.10	0.8
[Ru(bpy)$_2$dip]Cl$_2$ (B2D)	0.6	-0.30	0.9
[Ru(bpy)$_3$]Cl$_2$ (B3)	-2.1	-2.6	0.5

It is notable that the LogP$_{o/b}$ is always greater than the logP$_{o/w}$, with the minimum increase being 0.4. In fact, for all three homoleptic RPCs the ΔlogP is +0.4 to +0.5. At the simplest level, this difference can be attributed to a 'salting-out' of the lipophilic complex from the aqueous phase. Interestingly, the ΔlogP is substantially greater for all of the heteroleptic complexes, with values between +0.8 and +0.9 for [Ru(bpy)$_2$dip]Cl$_2$ and [Ru(dip)$_2$bpy]Cl$_2$ and values of +1.2 to +2.3 for [Ru(phen)$_2$dip]Cl$_2$ and [Ru(dip)$_2$phen]Cl$_2$. Under conditions in which there is ample chloride present, the dramatic increase in lipophilicity for [Ru(dip)$_2$phen]Cl$_2$ suggests something unusual is occurring, although we are not clear on what this is. This will be discussed in more detail later.

CHAPTER 3

Investigating the Cytotoxicity, Cellular Uptake, and Subcellular Localization of Ru(II)

Polypyridyl Complexes while Varying the Amount of Dip Ligands Coordinated

Introduction

In traditional drug development, drug lipophilicity is known to effect absorption rates, cellular uptake, and even subcellular distribution.[20-24,25] It has been noted that RPCs with higher lipophilicity are generally more cytotoxic. For instance, Mazuryk et al. compared the cytotoxic properties of several RPCs including $[Ru(dip)_2bpy]^{2+}$, $[Ru(dip)_2(CH_3bpy-CH_3)]^{2+}$, $[Ru(dip)_2(CH_3bpy-COO)]^+$, $[Ru(dip)_2(CH_3bpy-DCU)]^{2+}$, and $[Ru(dip)_2(bpy-NitroIm)]^{2+}$ on a 4T1 mouse breast cancer cell line.[14,25,26] The most cytotoxic of these was $[Ru(dip)_2(CH_3bpy-DCU)]^{2+}$ (4.71 µM IC_{50} value) which also had the highest $LogP_{o/w}$ 1.11.[25-26] Moreover, this complex also showed the highest cellular uptake as determined by flow cytometry using the luminescence of the RPC to quantify uptake.[25-26]

In this chapter, we report on the cytotoxicity, cellular uptake, and subcellular localization of MCF-7 and H-358 cells treated with the RPCs described in Chapter 2. As opposed to the determination of cellular uptake by fluorescent microscopy, we examined the ruthenium content in whole cells and cell lysates by ruthenium ICP-MS. The data are correlated with the RPC structure and the $LogP_{o/w}$ and $LogP_{o/b}$ data to delineate the role of lipophilicity and structure on performance. Another graduate student in the MacDonnell lab, Melissa Reardon M.S., was responsible for the synthesis and results of the phen based ruthenium complexes where my project stemmed from hers, where I synthesized the bpy based ruthenium complexes. Together, our complexes made up the family of RPCs seen throughout the entirety of this chapter.

<u>Experimental</u>

Chemicals

The source or preparation of [Ru(dip)$_3$]Cl$_2$, [Ru(dip)$_2$bpy]Cl$_2$, [Ru(bpy)$_2$dip]Cl$_2$, [Ru(dip)$_2$phen]Cl$_2$, [Ru(phen)$_2$dip]Cl$_2$, [Ru(bpy)$_3$]Cl$_2$, and [Ru(phen)$_3$]Cl$_2$, was described in Chapter 2. Dimethylsulfoxide was purchased from Sigma Aldrich and was used as received. A solution of 10 X phosphate buffered saline (PBS), pH 7.4 and 25 °C, was procured from Bio-Rad. The PBS had to be diluted before usage 10-fold using Millipore water resulting in a normal 1X PBS buffer. 1% penicillin/streptomycin, fetal bovine serum (FBS), DMEM-low glucose medium, RPMI-1640 medium, trypsin-EDTA (1X), and Trypan blue stain solution were all purchased from Sigma Aldrich. For the subcellular localization assay, a Qproteome Cell Compartment Kit was procured from Qiagen.

Cell Lines and Culture

The H-358 (human non-small cell lung carcinoma (NSCLC) bronchioalveolar) and MCF-7 (human epithelial cell adenocarcinoma) were obtained from University of Texas Southwestern Medical Center. Both cell lines were cultured in 60 mm culture plates in RPMI-1640 (for H-358) or DMEM (for MCF-7) with 10% FBS and 1% PS at 37°C and 5% CO$_2$ atmosphere with humidification.

Microwave Digestion Oven

Cellular uptake and subcellular fractionations were required to be digested in acid before being subjected to ICP-MS analysis. In order to accomplish this, the samples were placed in 0.5 mL deionized water then mixed with 4 mL of a 3.5 % nitric acid solution. This procedure was to be done in a Teflon-lined digestion vessel. A Mars5 XP-1500 microwave oven was employed to

digest the vessels with the samples being irradiated at 600 W at full power. The instrument was programed to reach 130 °C in a span of 5 minutes, then held at a constant 130 °C for another 5 minutes before cooling back down to room temperature. The samples within the digestion vessels were then transferred to a 15 mL centrifuge tube. The centrifuge tube was to be utilized as a storage vessel for when the samples are eventually analyzed by the ICP-MS. Upon transferring the samples to the centrifuge tube, up to 10 mL of 3.5 % nitric acid was used to dislodge the sample from the bottom of the digestion vessels. A total of 10 vessels could be placed in a run and each vessel had a membrane that was changed after each run. A control vessel was applied for each run to monitor the oven's temperature and pressure to guarantee if proper instrument parameters were being satisfied.

ICP-MS

Ruthenium determinations were obtained on an Agilent 7700 Series ICP-MS (single quadruple) instrument. The instrument was outfitted with an ASX-520 CETAC autosampler and MassHunter Workstation software was employed for data analysis. The parameters used to operate the instrument were as follows: Argon gas for cooling (13 L/min, auxiliary 0.8 L/min, nebulizer at 0.8 mL/min), RF power at 400 W, spray chamber temperature set at 3 °C, nickel interface cones, 1.9 mbar pressure in sample chamber, 3.60×10^{-7} mbar sample analyzing chamber, 150 mm sampling depth, detector mode set at pulse counting, ^{101}Ru element monitoring, 170 ms integration time. Before analyzing the samples, a 5-point calibration curve was used with the following concentrations: 8, 16, 32, 64, and 128 ppb. The linearity (R^2) value given by this calibration curve was routinely in the 0.96 to 0.98 region. All samples were run in triplicate in order to obtain averages and standard deviations.

MTT Cytotoxicity Assay

MTT (3-(4,5-Dimethylthiazol-2-yl)-2,5-diphenyltetrazolium bromide) is an indicator type assay that is used to measure the cytotoxicity of the RPCs.[6,7,14,17] This assay functions by subjecting the viable cells to the MTT indicator dye and converting this dye into formazan. The formazan is then able to crystalize within the solution, however, DMSO is then added to each well of the well-plate to solubilize the crystalized formazan resulting in a dark purple colored solution. Any possible dead cells cannot convert MTT to formazan therefore they cannot affect the results of the experiment. To determine the viable cell count, the absorbance must be recorded at 560 nm where formazan intensity directly corresponds to a feasible cell concentration. For a standard MTT assay, 10,000 cells of either MFC-7 or H-358 cell lines are seeded in each well of a 96 well-plate. These cells are then left to incubate for a period of 24 hours in an atmosphere of 5 % CO_2 at 37°C. Cells were treated with 0.01, 0.1, 1.0, 10, and 100 µM concentrations of the desired RPC for each test in triplicate. A control row and blank row were also utilized on the 96 well-plate but were treated with a 1 % v/v solution of DMSO. After cell treatment, the well-plate was incubated again for a period of 96 hours at 37°C. After 96 hours, the cells were treated with a 5 mg/ml solution of MTT. The MTT (30 µL) was added to each well in order to quantify the viable cell concentration. After the addition of the 30 µL MTT solution, the well-plate was again placed in the incubator at 37°C for a period of 4 hours. After 4 hours, the well-plates were shaken gently on an end-over-end shaker for 1 hour before being analyzed using a UV-Vis Plate Reader (BMG Labtech SPECTROstar Nano Microplate UV/VIS). The instrument was run at 560 nm with an automatic path length correction at 100 µL with no shaking.

The optical density values and the concentration of each complex provided via sigmoidal fits from the dose response curves, the IC_{50} values were able to be calculated. MTT assays were ran 5 times for each RPC utilized to ensure accurate results and standard deviations. The averages and standard deviations of the IC_{50} values are displayed below in Table 2.

Cellular Uptake Assay

The function of the cellular uptake experiments is to determine and quantify the amount of the ruthenium complex that enters the cell. Before conducting the experiment, 2 million H-358 and MCF-7 cancer cells were seeded on 60 mm cell culture plates. After seeding, the plates are left in an incubator for 24 hours at 37°C under a 5 % CO_2 atmosphere. A 2 mM stock solution of each ruthenium complex was prepared, and the cells were treated with 30 µL of this solution with the final concentration being 20 µM. Control plates were also seeded but the cells were treated with a 1 % v/v solution of DMSO. After treatment, the cells were incubated again at 37 °C under a 5 % CO_2 atmosphere for one hour. After one hour, the media in the 60 mm plates were removed, and washed 5 times with PBS. The cells are then trypsinized to dislodge them from the plate. The cells are then collected in a 15 mL centrifuge tube and centrifuged for 5 minutes. After the 5-minute centrifugation period, the cells form in a pellet formation at the bottom of the centrifuge tube, to which they are then resuspended and washed with PBS. The cells are then resuspended and washed 2 more time with PBS. The cell samples were then ready to be digested in the microwave oven, then analyzed via ICP-MS for their ruthenium content. The ensuing ruthenium content is reported in ng of Ru per one million cells.

Sub-Cellular Localization Assay

In order to fractionate the RPCs, a commercial Qproteome cell compartment assay kit was purchased. This assay is able to isolate four fractions of the cell which are the cytoskeleton, nuclear proteins, cytosol, and mitochondria/golgi apparatus/endoplasmic reticulum. The kit contains multiple buffers that aid in interacting with and extracting each cellular fraction with the help of varying temperatures. Before applying the Qproteome kit, 5 million cells of MCF-7 and H-358 cells were seeded on 60 mm cell culture plates. The plates were then incubated for a period of 24 hours at 37 °C under a 5 % CO_2 atmosphere. During this 24-hour period, a 2 mM stock solution of each Ru complex was made and used to treat the cells after the 24-hour period. Similar to the cellular uptake assay, control plates were used and treated with a 1 % v/v solution of DMSO with the overall final concentration of the seeded plates being 20 µM. Great care was taken to ensure the 2 mM Ru complex solution was uniformly distributed across the entire cell culture plate to guarantee accurate results. One hour after treatment, the media from the cell culture plate was removed and the cells were washed 5 times with PBS. After washing 5 times with PBS, the cells were then trypsinized and centrifuged for 5 minutes. The pellets were washed again with ice cold PBS for 3 times. The cells were then isolated to their respective fractions by utilizing the Qproteome kit. The cells were then counted using a hemocytometer coupled with a Trypan Blue staining protocol. The cell samples are then placed in 1.5 mL centrifuge tubes for storage and are then transferred to the digestion vessels. After microwave digestion, each fraction was analyzed via ICP-MS for their ruthenium content (ng).

Results and Discussion

As shown in Figure 6.1, the ruthenium uptake tends to increase with LogP (top LogP$_{o/w}$; bottom LogP$_{o/b}$) and we will argue shows a more consistent trend with the LogP$_{o/b}$ data over the LogP$_{o/w}$. The largest drop off in uptake occurs during the transition from RPCs with the general structure [Ru(dip)$_2$(L-L)]$^{2+}$ to [Ru(L-L)$_2$dip]$^{2+}$ (where L-L is bpy or phen), indicating the importance of possessing at least 2 dip ligands.
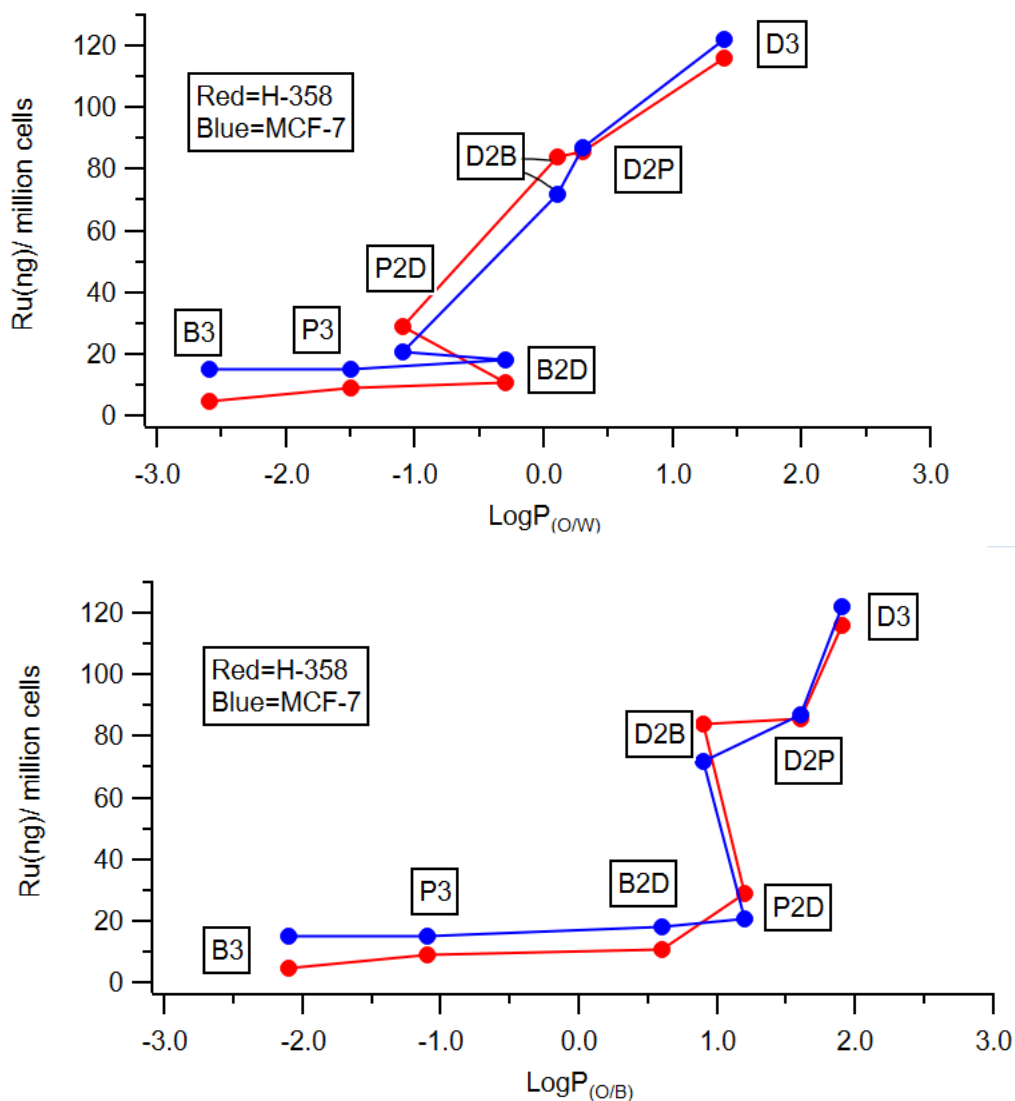
Figure 6.1. Correlation between LogP and Cellular Uptake for both MCF-7 and H-358 cell lines.
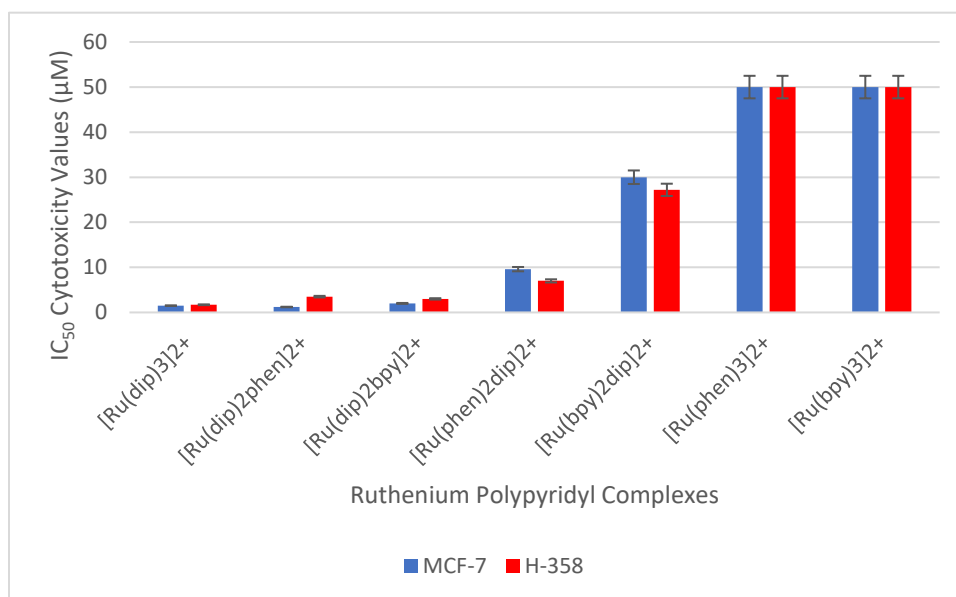
**Figure 6.2**. Cytotoxicity values of the synthesized RPC's where Series 1 (Blue) is the MCF-7 cell line and Series 2 (Red) is the H-358 cell line.

When plotted vs $LogP_{o/w}$ (Fig 6.1 (top)), ruthenium uptake is seen to increase substantially when $LogP_{o/w} > 0$, and there is slightly better uptake by P2D over B2D even though the P2D is nominally more hydrophilic. This gives rise to a zig-zag in the plot in which a more hydrophilic RPC shows better uptake. When this same data is plotted versus $LogP_{o/b}$, Ru uptake follows a more systematic increase with the LogP value, as the $LogP_{o/b}$ of $[Ru(phen)_2dip]^{2+}$ is now greater than $[Ru(bpy)_2dip]^{2+}$. Note that the $LogP_{o/b}$ values for $[Ru(phen)_2dip]^{2+}$ and $[Ru(dip)_2phen]^{2+}$ are similar, but the latter shows a 4-5 fold increase in ruthenium uptake. This shows that the molecular structure, and not simply the lipophilicity plays an important role in the ability of the RPC to cross the cell membrane. For whatever reason, the presence of two dip ligands dramatically improves uptake. Moreover, $[Ru(dip)_3]^{2+}$ shows even greater uptake which could be a function of the third dip ligand, the increase in $LogP_{o/b}$ or both.

The cytotoxicity of these RPCs also follows the $LogP_{o/b}$ data better than the $LogP_{o/w}$. Figure 6.2 shows a bar graph to the RPCs listed in order of decreasing $LogP_{o/b}$ versus cytotoxicity and it is clear that the cytotoxicity is highest for the more lipophilic RPCs and that the onset of cytotoxicity begins with $[Ru(bpy)_2dip]^{2+}$ which has a $logP_{o/b}$ of 0.6. The $[Ru(phen)_2dip]^{2+}$ is ~3 times more cytotoxic than the bpy homologue, which could be attributable to the slightly improved uptake. All RPCs containing two or more dip ligands show IC_{50}'s < 4 uM and only modest differences between them. This corresponds with the enhanced uptake seen once two dip ligands are present. The IC_{50} data was plotted versus the $LogP_{o/w}$ and o/b data, as shown in Figure 7 (top $LogP_{o/w}$; bottom $LogP_{o/b}$). Both plots show a zigzag about the $[Ru(phen)_2dip]^{2+}$ complex, but the magnitude of this anomaly is much smaller for the plot versus $LogP_{o/b}$. Again, we observe a threshold for the onset of activity near a $LogP_{o/b}$ of 1.0. The most compelling data is observed in Figure 8, which plots the IC_{50} values versus the ruthenium uptake.

Table 2. Entire family of RPCs with their respective cytotoxicity values and cellular accumulation. LogP is also displayed to better illustrate the correlation between cytotoxicity, uptake, and lipophilicity.

RPC	$LogP_{o/b}$	$LogP_{o/w}$	MCF-7: IC_{50} (µM)	H-358: IC_{50} (µM)	MCF-7: Uptake [Ru(ng)/cell (x10^6)]	H-358: Uptake [Ru(ng)/cell (x10^6)]
$[Ru(dip)_3]Cl_2$ (D3)	1.9	1.4	1.5 ± 0.3	1.7 ± 0.1	122 ± 3.6	116 ± 1.2
$[Ru(dip)_2phen]Cl_2$ (D2P)	1.6	0.3	1.2 ± 0.2	3.5 ± 0.2	87 ± 0.7	86 ± 1.6
$[Ru(dip)_2bpy]Cl_2$ (D2B)	0.9	0.1	2 ± 0.5	3 ± 0.5	72 ± 0.7	84 ± 0.8
$[Ru(phen)_2dip]Cl_2$ (P2D)	1.2	-1.1	9.6 ± 0.4	7.0 ± 0.3	21 ± 0.7	29 ± 0.2
$[Ru(bpy)_2dip]Cl_2$ (B2D)	0.6	-0.3	30 ± 2.4	27.2 ± 1.8	18 ± 3.1	11 ± 1.6
$[Ru(phen)_3]Cl_2$ (P3)	-1.1	-1.5	>50	>50	15 ± 0.8	9 ± 0.3
$[Ru(bpy)_3]Cl_2$ (B3)	-2.1	-2.6	>50	>50	15 ± 2.0	4.6 ± 0.3
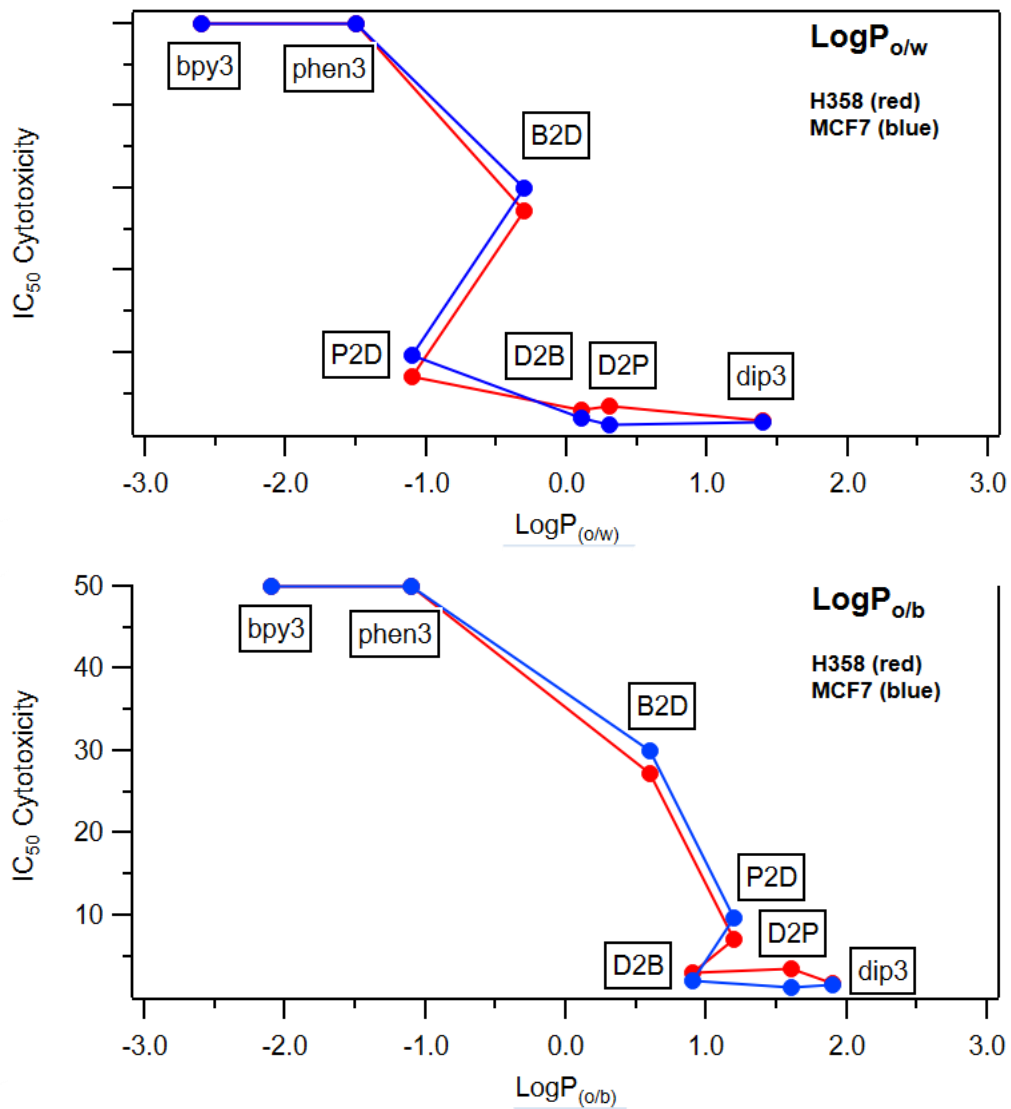
Figure 7. Correlation between LogP and IC_{50} cytotoxicity in MCF-7 and H-358 cell lines.
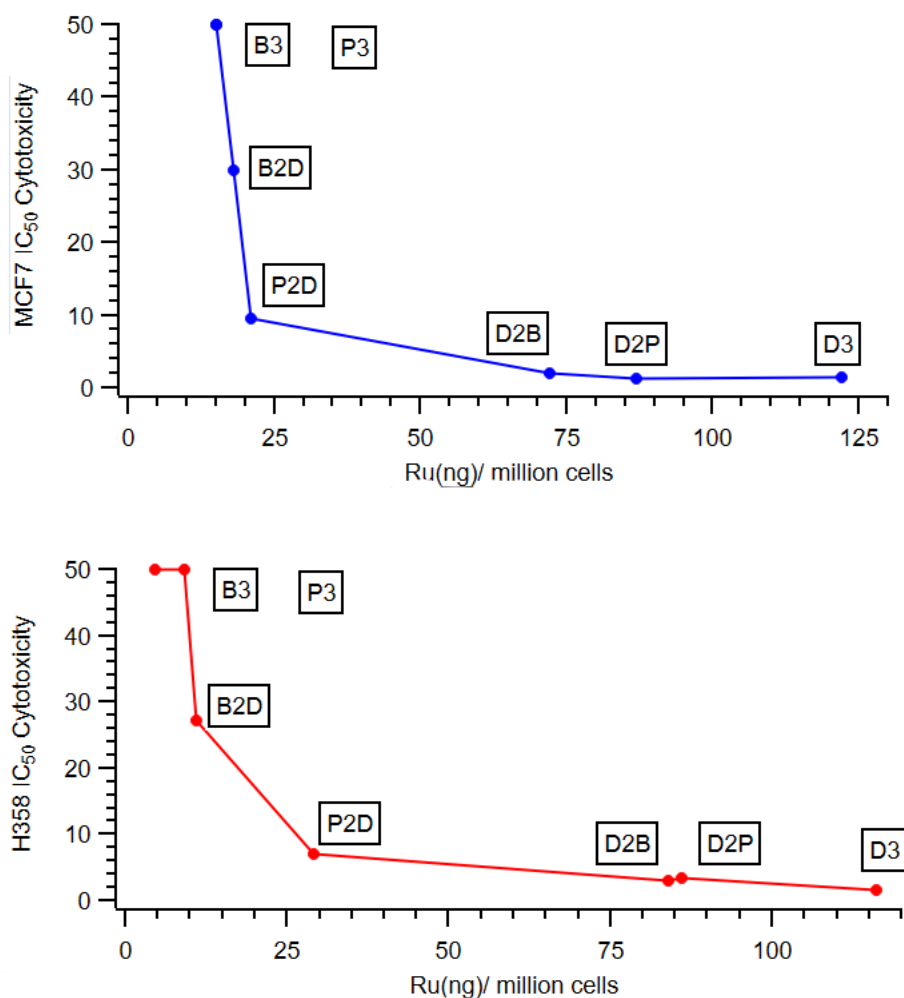
Figure 8. Correlation between cellular uptake versus IC_{50} cytotoxicity in both MCF-7 and H-358 cell lines.

Based on Figure 8, we can see that there is one less data point on the MCF-7 plot compared to the H-358 plot. This is due to B3 and P3 having the exact same amount of cellular uptake. For both cell lines, around 20-30 ng of ruthenium is needed to have a decent cytotoxicity. This can be seen in the B2D and the P2D points. Having any cellular uptake amount greater than 30 ng makes the complexes extremely cytotoxic as seen for the D2B, D2P and D3 points. The

shape of both graphs both resemble plots of exponential decay, yet you still have to take into

account the B3 and P3 points are only plotted at 50 µM. Their true IC_{50} values are closer the 100

µM mark.

Previously, other groups studying the subcellular localization of RPCs, specifically

[Ru(dip)$_3$]Cl$_2$, have discovered that mitochondria is the subcellular target of this particular

RPC.[25,26,39,48,49] Based on the data shown in Figures 9 and 10, this is not the case. The data shown

below indicates that the RPCs synthesized target the cytoskeletal proteins of the treated cells. A

possible reason for this discrepancy between results could be the differing cell lines. It may very

well be that cell lines such as MCF-7 and H-358 may have more of an affinity of RPCs

accumulating in its cytoskeleton while other cell line such as A-549 have RPCs accumulate in its

mitochondria. Another factor that needs to be considered between the data below and others'

research results is the type of assay conducted. The assay typically conducted in other subcellular

localization studies involves the use of microscopy and luminescence used in conjunction with

dyes, such as Mitotracker Green.[26] These three factors are combined and utilized together to

show where the RPC typically congregates within an organelle.[26] This approach only focuses on

highly luminescent areas of high concentration and does not factor in the type of environment the

RPC is localized in. We applied the use of a QIAGEN compartmentalization kit that was able to

fractionate the treated cells into four different organelles by using its differing buffers and

following its procedure. After these proteinaceous components were separated, the samples were

then digested via microwave oven, then analyzed via ICP-MS for their respective whole cell Ru

content.
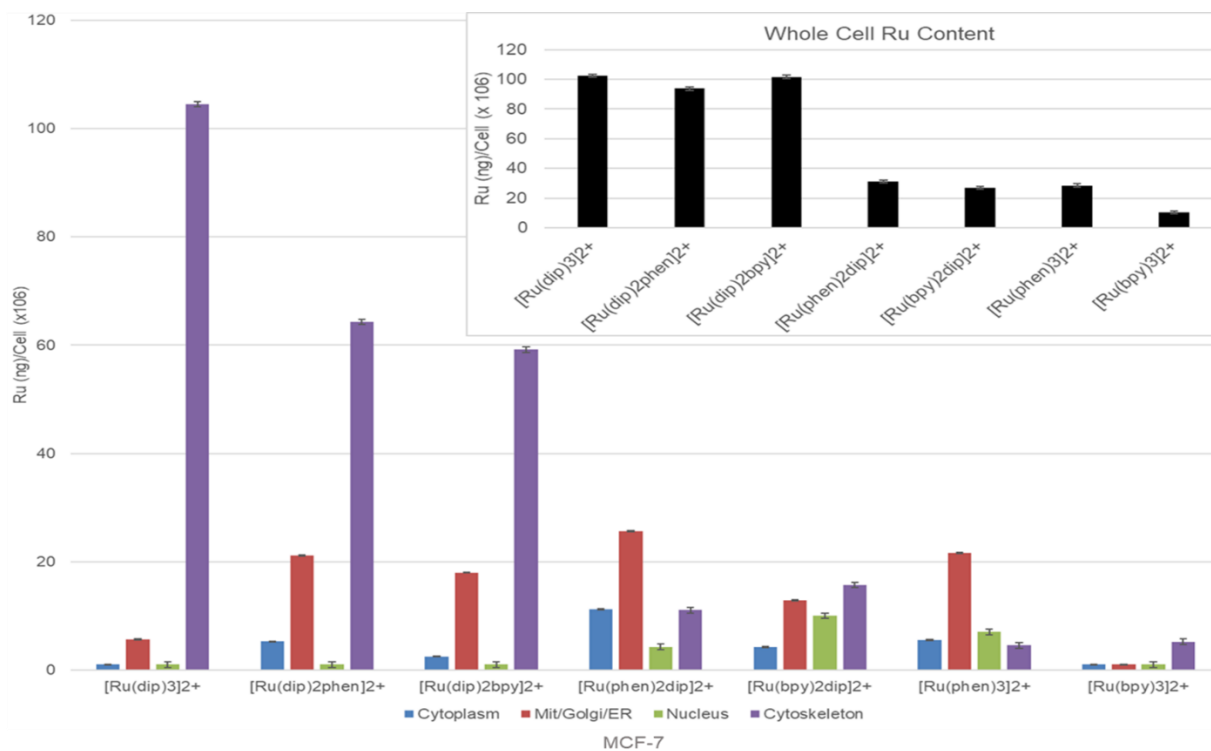
Figure 9. Subcellular localization data of the treated MCF-7 cell line. Displays the Ru content from the family RPCs in ng per one million cells. Obtained by utilizing the Qiagen protocol which separates the cellular organelles into the nucleus, mitochondria/ER/golgi, cytoskeleton, and cytosol. Cellular uptake results are also displayed to better observe the total Ru mass accumulated for the MCF-7 cell line.
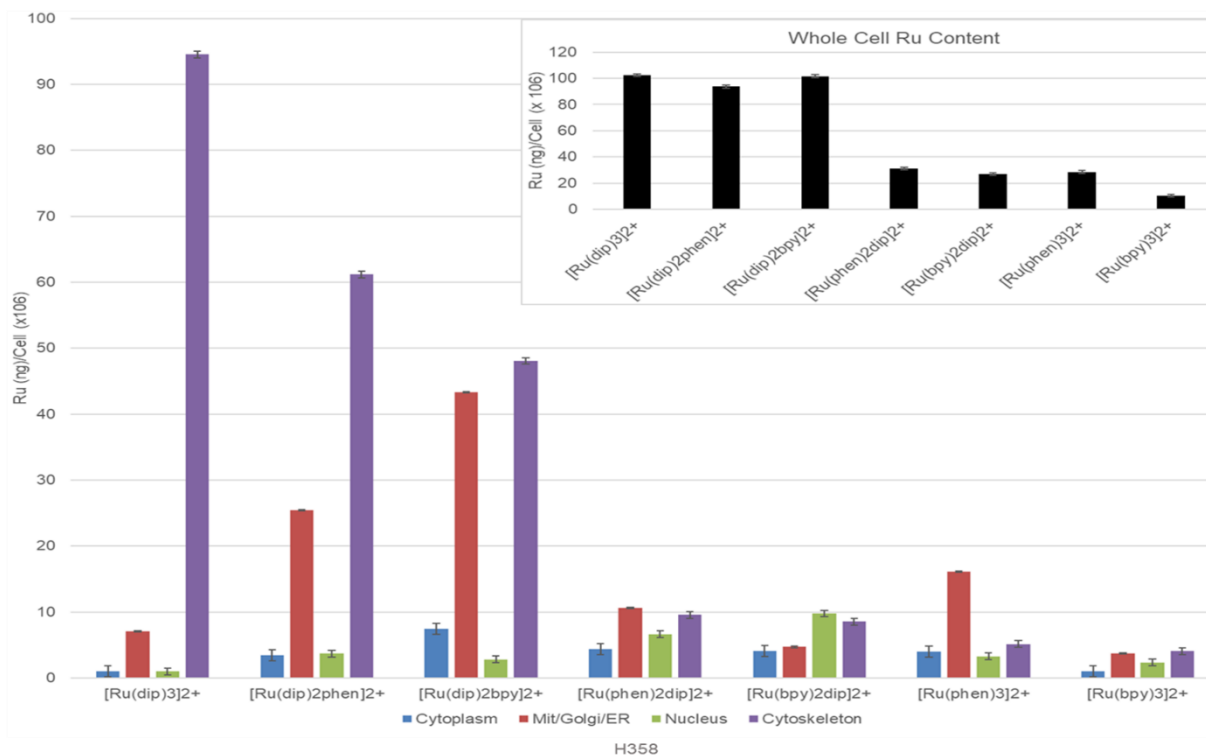
Figure 10. Subcellular localization data of the treated H-358 cell line. Displays the Ru content from the family RPCs in ng per one million cells. Obtained by utilizing the Qiagen protocol which separates the cellular organelles into the nucleus, mitochondria/ER/golgi, cytoskeleton, and cytosol. Cellular uptake results are also displayed to better observe the total Ru mass accumulated for the H-358 cell line.

The data presented in the bar graphs above shows where the family of Ru complexes tends to target in MCF-7 and H-358 cell lines, respectively. The whole cell ruthenium content was added to each of the two figures above for the purpose of data correlation. This aids in viewing how much of a factor the lipophilicity is when determining how cellular uptake correlates with the subcellular localization. The figures above illustrate the distributions of the RPCs in the four different cellular organelles. The cytosolic proteins are shown in blue, the mitochondrial proteins are shown in red, the nucleus is represented in green, and the cytoskeletal components are exhibited in purple. The two least lipophilic complexes, $[Ru(bpy)_3]Cl_2$ and $[Ru(bpy)_2dip]Cl_2$, have a more uniform distribution across the four cellular fractions, especially

for the H-358 cell line, however, these two particular complexes have the least uptake across both cell lines. The three most uptaken complexes across both cell lines, $[Ru(dip)_3]Cl_2$, $[Ru(dip)_2phen]Cl_2$, and $[Ru(dip)_2bpy]Cl_2$, are the most lipophilic as well. $[Ru(dip)_3]Cl_2$ has a stronger presence in the cytoskeleton out of the other three cellular fractions, typically having 95-105 ng per million cells. The other more lipophilic complexes, $[Ru(dip)_2bpy]Cl_2$ and $[Ru(dip)_2phen]Cl_2$, also localize in the cytoskeleton while also having some distribution in the mitochondria especially in the H-358 cell line. This type of localization shift from hydrophilic to lipophilic complexes to congregate more in the cytoskeletal components compares well with the cellular uptake and the cytotoxicity data. One minor discrepancy between the data is the difference between the cell lines for the compartmentalization assay. In the MCF-7 cell line, $[Ru(dip)_2bpy]Cl_2$ has a clear affinity for the cytoskeleton with minimal affinity for the other cellular proteins with a minimal affinity for the mitochondria. In the H-358 cell line that is not the case as there is a greater affinity to target the mitochondria compared to the MCF-7 cell line. Nevertheless, $[Ru(dip)_2bpy]Cl_2$ still has more affinity to target the cytoskeleton in H-358 but not as much as MCF-7, as it is also distributed more in the mitochondria. We can presume that, as long as there are two dip ligands coordinated to our complex, we can easily target the cytoskeleton. However, anything less than two dip ligands trends toward the mitochondria. For H-358, this trend holds true here as well.

Conclusion

We have synthesized a family of RPCs with the dip, bpy, and phen ligands. The main premise of the relationship between this family of RPCs is by altering the dip ancillary ligands to bpy/phen and vice versa. For this family, the dip ligand is extremely useful in providing high lipophilicity throughout the entire complex. The bpy/phen ligands are utilized for their enhanced solubility. It is needed due to the homoleptic Ru complex, $[Ru(dip)_3]Cl_2$, being insoluble in water. In order to conduct lipophilicity and biological assays, this homoleptic complex needed to be dissolved in DMSO then diluted with water to be used in these assays. As a result of alternating one and two dip ancillary ligands from the $[Ru(dip)_3]Cl_2$ complex, the four derivatives $[Ru(dip)_2bpy]Cl_2$, $[Ru(bpy)_2dip]Cl_2$, $[Ru(dip)_2phen]Cl_2$, $[Ru(phen)_2dip]Cl_2$ were synthesized. These four complexes remained lipophilic but also possessed improved water solubility which was crucial for their usage in biological assays. This water solubility highlights the hydrophilic properties of the bpy and phen ligands as well, however, the $[Ru(dip)_2phen]Cl_2$ complex required slight sonication before completely dissolving in solution, while $[Ru(dip)_2bpy]Cl_2$ can be freely dissolved in aqueous solutions. Throughout the cytotoxicity, cellular uptake, and subcellular localization assays, the dip ligand contributed a vital role in biological activity and a patter was established in each of these assays. This pattern is better highlighted in the $[Ru(dip)_2bpy]Cl_2$ and $[Ru(dip)_2phen]Cl_2$ complexes as their relationship between lipophilicity and cellular uptake was emphasized above in Figure 6.1 which enabled us to visualize an optimal range for LogP forming between 0 and 1. It was in this range where we can see D2B and D2P uptake values skyrocket into the 80 ng range for cellular uptake. These complexes also had elevated cytotoxicity values (2-3 uM) while having accumulated higher cellular uptake values and consistently targeting the cytoskeletal proteins regardless of cell line

used. Upon examination of Tables 1 and 2, as well as Figure 7, the data shown for $LogP_{o/b}$ can be seen as superior to the data of $LogP_{o/w}$. For Figure 7 specifically, the data shows a more linear trend with $LogP_{o/b}$ compared to the trend seen with the data from $LogP_{o/w}$, even with the P2D complex being the main outlier as it shifts from an o/b solution to an o/w solution. LogP is most commonly reported in octanol/water, however $LogP_{o/b}$ can be influenced by the salination of the buffer system in use. In the body, cells as well as blood can be seen as buffered systems so the counterion our complexes utilize have a strong influence on solubility. Therefore, we can conclude that the $LogP_{o/b}$ data can be more beneficial.

Due to the promising nature of the $[Ru(dip)_2bpy]Cl_2$ and $[Ru(dip)_2phen]Cl_2$ complexes, more research is needed to ascertain the targeting of the cytoskeletal components. Upon comparison of the two most promising complexes synthesized, $[Ru(dip)_2bpy]Cl_2$ and $[Ru(dip)_2phen]Cl_2$, one can notice the striking similarities both of these complexes exhibit in terms of LogP, cytotoxicity and cellular uptake. However, if one were to choose the most promising complex to continue forward with, the $[Ru(dip)_2bpy]Cl_2$ would be a better option due to its freely solubilizing nature in water; as $[Ru(dip)_2phen]Cl_2$ required some sonication in order to completely dissolve in water. Additional studies of this kind could bring about new and improved metal-based complexes that could also target the cytoskeleton and microtubules in cancer cells.

References

1. Tong, M.Y. Payagala, T. Perera, S. MacDonnell, F. Study of a new chiral selector: Sodium arsenyl-(L)-(+) tartrate for capillary electrophoresis. *J. of. Chrom*. **2009**. 1217 (7):1139-48

2. J. H. Koch, W. P. Rogers, F. P. Dwyer and E. C. Gyarfas, Aust. *J. Biol. Sci.*, **1957**, 10, 342–350

3. A. E. Friedman, J. C. Chambron, J. P. Sauvage, N. J. Turro and J. K. Barton, Dywer, J. *J. Am. Chem. Soc*.**1990**, 112, 4960–4962

4. Puckett, C.; Barton, J.; Methods to Explore Cellular uptake of Ruthenium Complexes. *J. Am. Chem. Soc*. **2007**, 129, 46−47.

5. Dayoub, Adam PhD. Dissertation, Intracellular Biochemical Targets of Ruthenium Polypyridyl Complexes in Multiple Cancer Cell Models. The University of Texas at Arlington, Arlington, Tx. **2016**.

6. Alatrash, N.; Narh, E.; Yadav, A.; Kim, M.; Janaratne, T.; Gabriel, J.; MacDonnell, F.; Synthesis, DNA Cleavage Activity, Cytotoxicity, Acetylcholinesterase Inhibition, and Acute Murine Toxicity of Redox-Active Ruthenium(II) Polypyridyl Complexes. *Chem. Med. Chem* **2017**, *12*, 1055–1069.

7. Alatrash, N. MS Thesis. Increasing lipophilicity of redox active Ruthenium complexes as a means to enhance cytotoxicity and reduce animal toxicity. The University of Texas at Arlington, Arlington, TX, **2012**.

8. Fujita, T.; Iwasa, J.; Hansch, C.; A New Substituent Constant, π, Derived from Partition Coefficients. *J. Am. Chem. Soc.* **1964**, *86* (23), 5175–5180.

9. Altmann, K. H., Microtubule-stabilizing agents: a growing class of important anticancer drugs. *Curr. Opin. Chem. Biol.* **2001**, *5* (4), 424–431.

10. Sullivan, B.; Salmon, D.; Meyer, T. Mixed phosphine 2,2'-bipyridine complexes of ruthenium. *Inorg. Chem.* **1978**, *17* (12), 3334-3341.

11. Hartshorn, R.; Barton, J. Novel dipyridophenazine complexes of ruthenium(II): exploring luminescent reporters of DNA. J. Am. Chem. Soc. **1992**, 114 (15), 5919-5925.

12. McFarland, S. A. Mandel, A. Dumoulin-White, R. Gasser, D. Metal-based Photosensitizers for Photodynamic Therapy: The Future of Multimodal Oncology. *Curr. Opin. Chem. Biol*. **2020**. 56:23-27.

13. Zava, O.; Zakeeruddin, S. M.; Danelon, C.; Vogel, H.; Grätzel, M.; Dyson, P. J., A Cytotoxic Ruthenium Tris(Bipyridyl) Complex that Accumulates at Plasma Membranes. *Chem. Bio. Chem.* **2009**, *10* (11), 1796–1800.

14. Alessio, E; Messori, L. NAMI-A and KP1019/1339, Two Iconic Ruthenium Anticancer Drug Candidates Face-to-Face: A Case Story in Medicinal Inorganic Chemistry. *Molecules*. **2019**, 24 (10), 1995.

15. Mazuryk, O. Magiera, K. Rys, B. Suzenet, F. Kieda, C. Brindell, M. Multifaceted interplay between lipophilicity, protein interaction and luminescence parameters of non-intercalative ruthenium(II) polypyridyl complexes controlling cellular imaging and cytotoxic properties. *J. Biol. Inorg. Chem*. **2014**, 19(8): 1305–1316.

16. Varbanov, H. Kuttler, F. Banfi, D. Turcatti, G. Dyson, P. Screening-based approach to discover effective platinum-based chemotherapies for cancers with poor prognosis. *PLoS 1*. **2019**, 14(1): e0211268.

17. Dickerson, M. Sun, Y. Howerton, B. Glazer, E. Modifying Charge and Hydrophilicity of Simple Ru(II) Polypyridyl Complexes Radically Alters Biological Activities: Old Complexes, Surprising New Tricks. *J. Inorg. Chem*. **2014**, 53, 10370-10377.

18. Alastrash, N. Issa, F. Bawazir, N. West, S. Van-Mannen Brush, K. Shelor, P. Dayoub, A. Myers, K. Janetopoulos, C. Lewis, E. MacDonnell, F. Disruption of microtubule function in cultured human cells by a cytotoxic ruthenium(II) polypyridyl complex. *Chem. Sci.*, **2020**, 11, 264.

19. QIAGEN. Qproteome® Cell Compartment Handbook. https://www.qiagen.com_preHB_Qproteome_Cell_Compartment_20121023.pdf (accessed May 23, 2021)

20. Stordal, B. Davey, M. Critical Review Understanding Cisplatin Resistance Using Cellular Models. *Life*. **2007**, 59 (11), 696–699.

21. Chen, S. Chang, J. New Insights into Mechanisms of Cisplatin Resistance: From Tumor Cell to Microenvironment. *Int. J. Mol. Sci*. **2019**, 20 (17), 4136–4157.

22. Karahalil, B. Yardim-akaydin, S. Baytas, S. An Overview of Microtubule Targeting Agents for Cancer Therapy. *Arh. Hig. Rada. Toksikol*. **2019**, 70 (5), 160–172.

23. Pisani, M. Fromm, P. Mulyana, Y. Clarke, R. Korner, H. Heimann, K. Collins, J. Keene, F. Mechanism of Cytotoxicity and Cellular Uptake of Lipophilic Inert Dinuclear Polypyridylruthenium(II) Complexes. *Chem. Med. Chem*. **2011**. 6 (5), 848–858.

24. Einstein A. The First Microtubule Stabilizing Agent Taxol. *Int. J. Mol. Sci*. **2017**, 18, 2-11.

25. Stanton, R. Gernert, K. Nettles, J. Aneja, R. Drugs that Target Dynamic Microtubules: A New Molecular Perspective. *Med. Res. Rev*. **2011**, 31(3), 443-481.

26. Mazuryk, O. Magiera, K. Multifaceted Interplay between Lipophilicity , Protein Interaction and Luminescence Parameters of Non-Intercalative Ruthenium (II) Polypyridyl Complexes Controlling Cellular Imaging and Cytotoxic Properties. *J. Biol. Inorg. Chem.* **2014**, 19, 1305-1316.

27. Mazuryk, O. Kurpiewska, K. Lewinski, K. Stochel, G. Brindell, M. Interaction of apo-transferrin with anticancer ruthenium complexes NAMI-A and its reduced form. *J. Inorg. Biochem.* **2012**, 116: 11-8.

28. Vargui, A.V. Robertazzi, A. Magistrato, A. Ruggerone, P. Carloni, P. The hydrolysis mechanism of the anticancer ruthenium drugs NAMI-A and ICR investigated by DFT-PCM calculations. *J. Phys. Chem.* **2008**, 112 (14): 4401-4409.

29. Ravera, M. Baracco, S. Cassino, C. Zanello, P. Osella, D. Appraisal of the redox behaviour of the antimetastatic ruthenium(III) complex [ImH][RuCl(4)(DMSO)(Im)], NAMI-A. Dalton Trans. 2004, 15: 2347-2351.

30. Groessel, M. Reisner, E. Hartinger, C.G. Eichinger, R. Semenova, O. Timerbaev, A.R. Jakupec, M.A. Arion, V.B. Keppler, B.K. Structure-activity relationships for NAMI-A-type complexes (HL)[trans-RuCl4L(S-dmso)ruthenate(III)] (L = imidazole, indazole, 1,2,4-triazole, 4-amino-1,2,4-triazole, and 1-methyl-1,2,4-triazole): aquation, redox properties, protein binding, and antiproliferative activity. *J. Med. Chem.* **2007**, 50(9): 2185-2193.

31. Alessio, E. Mestroni, G. Bergamo, A. Sava, G. Ruthenium metastatic agents. *Curr. Top. Med. Chem.* **2004**, 4(15): 1525-1535.

32. Bergamo, A. Sava, G. Ruthenium targets can target determinants of tumor malignancy. *Dalton. Trans.* **2007**, (13): 1267-1272.

33. Gill, M. Derrat, H. Smythe, C. Battalgia, G. Thomas, J. Ruthenium(II) metallo-intercalators: DNA imaging and cytotoxicity. *Chem. Biochem*. **2011**, 12: 877-880.

34. Gao, F. Chao, H. Zhou, F. Yuan, Y. Peng, B. Ji, L. DNA interactions of a functionalized ruthenium(II) mixed-polypyridyl complex [Ru(bpy)2ppd]2+. *J. Inorg. Biochem*. **2006**, 100: 1487-1494.

35. Rathinasamy, S. Karki, S. Bhattacharya, S. Mankidan, L. Prabakaran, S. Gupta, M. Mazumder, U. Synthesis and anticancer activity of certain mononuclear Ru (II) Complexes. *J. Enzyme. Inhib. Med. Chem*. **2006**, 21 (5), 500-508.

36. Lippert, B. Cisplatin: Chemistry and Biochemistry of a Leading Cancer Drug. Wiley-VCH: Weinhein, 1999.

37. Dwyer, F. Gyarfas, E. Rogers, W. Koch, J. Biological Activity of Complex Ions. *Nature*. **1952**, 170, 190-192.

38. Tan T. Weston, H. Hogan, J. *Int. J. Appl. Radiat. Isot*. **1971**, 22 (5), 300-308.

39. Wilson, J. Lippard, J. Synthesis Characterization and Cytotoxicity of Platinum (IV) Carbamate Complexes. *J. Med. Chem*. **2012**, 55 (11), 5325-5335.

40. Puckett, C. A. Exploring the cellular accumulation of metal complexes. *Dalton Transactions*. **2010**. 39(5): 1159-1170.

41. Gao, F. DNA Binding, Photocleavage, and Topoisomerase Inhibition of Functionalized Ruthenium(II)-Polypyridine Complexes. *Chemistry & Biodiversity*. **2008**. 5(10): 1962-1979.

42. Pyle, A. M.; J. K. Barton Probing nucleic acids with transition metal complexes. *Prog. Inorg. Chem. S. J. Lippard. New York, John Wiley and Sons, Inc*. **1990**. 18: 413-476.

43. Griffith, C. Cellular and cell-free studies of catalytic DNA cleavage by ruthenium polypyridyl complexes containing redox-active intercalating ligands. *Chem. Sci.* **2017**. 8(5): 3726-3740.

44. Notaro, A.; G. Gasser. Monomeric and dimeric coordinatively saturated and substitutionally inert Ru(ii) polypyridyl complexes as anticancer drug candidates. *Chem. Soc. Rev.* **2017**. 46(23): 7317-7337.

45. Poynton, F. E. The development of ruthenium(ii) polypyridyl complexes and conjugates for in vitro cellular and in vivo applications. *Chem. Soc. Rev*. **2017**. 46(24): 7706-7756.

46. Li, X. Kinetically-inert polypyridylruthenium (II) complexes as therapeutic agents. *Coord. Chem. Rev*. **2018**. 375: 134-147.

47. Babu, E. Unravelling the aggregation induced emission enhancement in Tris(4,7-diphenyl-1,10-phenanthroline)ruthenium(II) complex. *Inorg. Chem. Comm*. **2018**. 98: 7-10.

48. Pierroz, V. Molecular and Cellular Characterization of the Biological Effects of Ruthenium(II) Complexes Incorporating 2-Pyridyl-2-pyrimidine-4-carboxylic Acid. *J. Am. Chem. Soc*. **2014**. 134(50): 20376-20387.

49. Pisani MJ, W. D., Heimann K, Collins JG, Keene FR. Selective mitochondrial accumulation of cytotoxic dinuclear polypyridyl ruthenium(II) complexes. *Metallomics*. **2010**. 2: 393-396.

50. Chen, T. Ruthenium Polypyridyl Complexes That Induce Mitochondria-Mediated Apoptosis in Cancer Cells. *Inorg. Chem*. **2010**. 49(14): 6366-6368.

51. Shum, J. Luminescent Ruthenium(II) Polypyridine Complexes for a Wide Variety of Biomolecular and Cellular Applications. *Inorg. Chem*. **2019**. 58(4): 2231-2247.
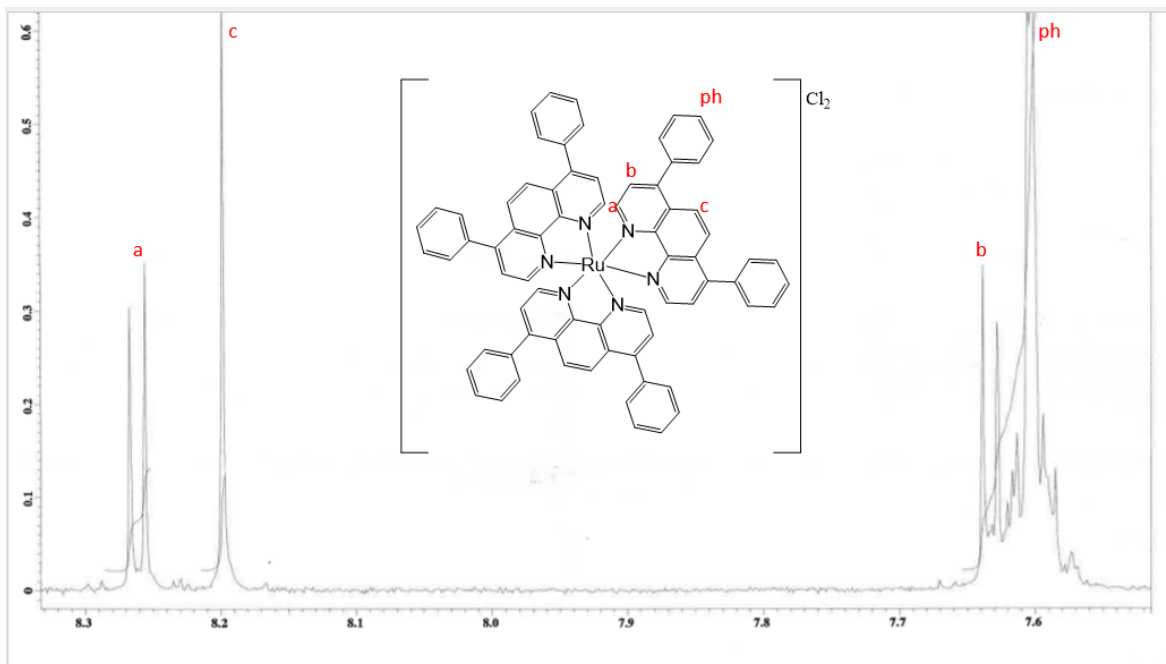
Appendix

A. Additional NMR Data

Figure A1. ^{1}H NMR labeling of the [Ru(dip)$_3$]$^{2+}$ complex. Ph represents the phenyl group attached to the dip ligand. Letters a-c represent the dip ligand protons.
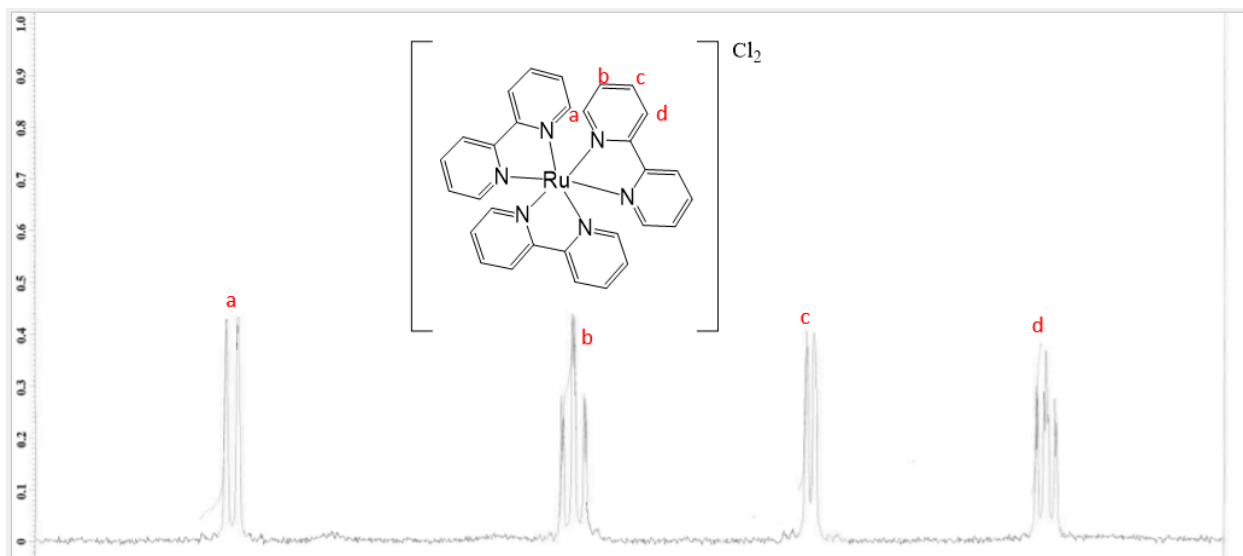
Figure A2. ^{1}H NMR labeling of the $[Ru(bpy)_3]^{2+}$ complex. Letters a-d represent the bpy ligand protons.